IEEE Photonics Journal
An IEEE Photonics Society Publication

Open Access

# Reduced Graphene Oxide/Maghemite Nanocomposite for Detection of Lead Ions in Water Using Surface Plasmon Resonance

Volume 10, Number 6, December 2018

Ali Abdulkhaleq Abdulhadi Alwahib
Yasmin Mustapha Kamil
Muhammad Hafiz Abu Bakar
Ahmad Shukri Muhammad Noor
Mohd Hanif Yaacob
Hong Ngee Lim
Nay Ming Huang
Mohd Adzir Mahdi

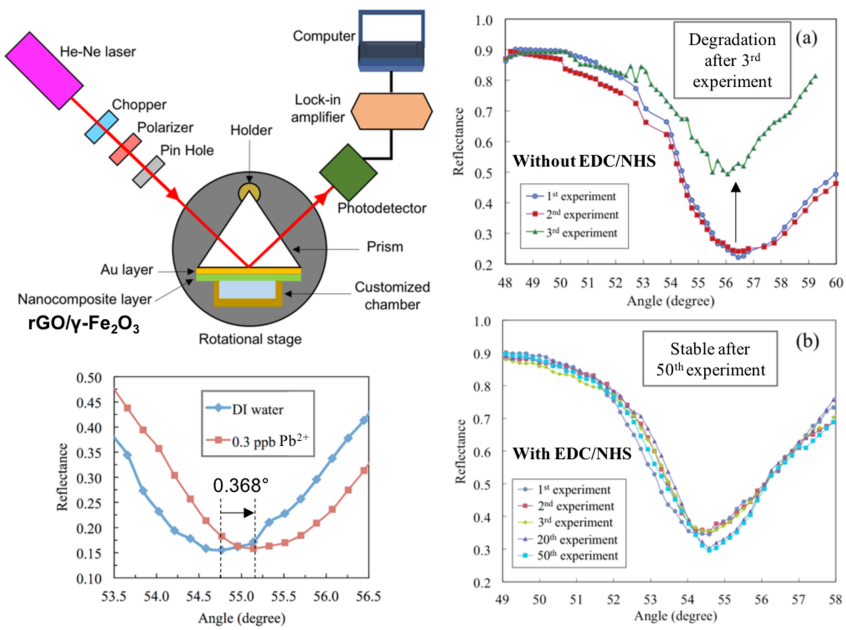


DOI: 10.1109/JPHOT.2018.2877190
1943-0655 © 2018 IEEE

# Reduced Graphene Oxide/Maghemite Nanocomposite for Detection of Lead Ions in Water Using Surface Plasmon Resonance

**Ali Abdulkhaleq Abdulhadi Alwahib,[1,2] Yasmin Mustapha Kamil,[2] Muhammad Hafiz Abu Bakar,[2] Ahmad Shukri Muhammad Noor,[2] Mohd Hanif Yaacob,[2] Hong Ngee Lim,[3] Nay Ming Huang,[4] and Mohd Adzir Mahdi [2]**

[1]Department of Laser and Optoelectronics Engineering, University of Technology, Baghdad 35010, Iraq
[2]Wireless and Photonics Network Research Centre, Faculty of Engineering, Universiti Putra Malaysia, Serdang 43400, Malaysia
[3]Department of Chemistry, Faculty of Science, Universiti Putra Malaysia, Serdang 43400, Malaysia
[4]Faculty of Engineering, Xiamen University of Malaysia, Sepang 43900, Malaysia

*DOI:10.1109/JPHOT.2018.2877190*
*1943-0655 © 2018 IEEE. Translations and content mining are permitted for academic research only. Personal use is also permitted, but republication/redistribution requires IEEE permission. See http://www.ieee.org/publications_standards/publications/rights/index.html for more information.*

Manuscript received August 23, 2018; revised October 2, 2018; accepted October 5, 2018. Date of publication October 22, 2018; date of current version November 13, 2018. This work was supported by the Ministry of Education Malaysia under Grant FRGS/2/2014/TK03/UPM/01/1. Corresponding author: M. A. Mahdi (e-mail: mam@upm.edu.my).

**Abstract:** A prism-based surface plasmon resonance (SPR) sensor deposited with reduced graphene oxide/maghemite is presented for the detection of lead ions ($Pb^{2+}$) in water. The SPR setup proposed followed the Kretschmann configuration with the installment of the nanocomposite integrated bilayer sensor chip onto the prism. For protection, the nanocomposite active layer was coated with 1-ethyl-3-(3-dimethylaminopropyl) -carbodiimidehydrochloride/N-hydroxysuccinimide. When the sensor was tested with different concentrations of $Pb^{2+}$ in static water, the limit of detection was achieved at 0.001 ppm with a resonance angle shift of 0.184°. As an improvisation, a sample circulation design was adapted into the setup in order to increase the interaction rate between the sample and the sensing layer. This managed to improve the detection limit to 0.3 ppb.

**Index Terms:** Optical sensing and sensors, surface plasmon, graphene.

## 1. Introduction

Lead ($Pb^{2+}$) has been identified by the World Health Organization to be among the top 10 chemicals of major public health concern. At very minute concentrations, $Pb^{2+}$ has the potential to cause severe damage to the nervous system which may lead to deaths. Based on data collected in 2015 by Institute for Health Metrics and Evaluation, $Pb^{2+}$ exposure had caused 494,550 deaths and 9.3 million disability adjusted life years due to long-term effects [1]. Among the preventative steps taken to tackle the crisis is by developing reliable sensing systems which are cost effective, easily accessible, and reliable. To date, various techniques have been used which include fluorimetry, colorimetry, graphite furnace atomic absorption spectrometry and mass spectrometry [2]. However, these techniques are laborious, time-consuming and expensive.

TABLE 1
SPR-Based Sensors for the Detection of $Pb^{2+}$

| Ref. | Sensing layer | LOD |
|---|---|---|
| [3] | Chitosan/Graphene oxide | 30 ppb |
| [9] | Polypyrole-multi-walled carbon nanotube | 100 ppb |
| [10] | Silver/Gold/Chitosan-Graphene | 100 ppb |
| [11] | Molecular imprinted polymer (Methacrylic acid, 2,2-azo-bis-isobutyronitrile, trimethylolpropane trimethacrylate) | 100 ppb |
| [12] | Chitosan/Graphene oxide | 1 ppb |

The implementation of surface plasmon resonance (SPR) in sensor systems has been acknowledged as an enticing diagnostic technique for both biological and chemical specimens. The working principle of SPR sensors are based on the interaction of electrons oscillating on the metal-external medium interface with changes occurring in the external media, as they travel in parallel with the surface. Among the different SPR configurations that have been reported include prism-based [3], fiber-based [4], and waveguide-coupled based SPR [5]–[8]. In the past decade, researchers have dedicated their time towards investigating the incorporation of nanomaterials onto the SPR interfaces and the effects towards the performance of the sensor. A previous study reported the use of chitosan-graphene oxide composite as a sensing layer to a prism-based SPR setup for $Pb^{2+}$ detection which obtained a limit of detection (LOD) as low as 1 ppb. Other recent reports using nanomaterials as sensing layers for the detection of $Pb^{2+}$ are listed in Table 1.

Among the nanomaterials that were thoroughly investigated were carbon-based compounds like graphene and its derivatives. Reduced graphene oxide (rGO) has exhibited remarkable mechanical, thermal, electrical properties with very high surface to volume ratio. Not only that, due to its honeycomb mesh structure which is abundant with functional groups, rGO has been regarded as a great adsorbent [13]. Aside from that, the modification of rGO with paramagnetic nanoparticles, such as maghemite ($\gamma$-$Fe_2O_3$) was found to have significant affinity towards heavy metals due to the magnetic properties of the maghemite [14]. A study was previously reported to have been successful in detecting and removing Arsenic from ground water using rGO/$\gamma$-$Fe_2O_3$ nanocomposite [13]. It is very much likely that the same nanocomposite could yield similar results in detecting $Pb^{2+}$. However, to the best of our knowledge, such a method for $Pb^{2+}$ detection has yet to be reported.

In this work, the detection of $Pb^{2+}$ in aqueous solution was conducted using rGO/$\gamma$-$Fe_2O_3$ nanocomposite as a sensing layer to a prism-based SPR sensor. A layer of 1-ethyl-3-(3-dimethylaminopropyl)-carbodiimidehydrochloride/N-hydroxysuccinimide (EDC/NHS) was added on the sensing layer to enhance the integrity of the nanocomposite. Enhancement to the LOD and response time was achieved through integration of water circulation system.

## 2. Experimental Setup

The prism-based SPR used throughout this work followed the Krestchmann configuration as exhibited in Fig. 1. Firstly, light was emitted from a Helium-Neon (HeNe) laser at wavelength $\lambda = 633$ nm into a chopper plate, a transverse magnetic polarizer and a pinhole before coupling into a glass prism ($n = 1.779$) that was placed on a rotational stage (Sigma Koki SGSP-60YAW). The rotational stage with its motor controller (Newport NM 3000) enables full control over the incident angle of the laser beam as it hits the prism. The base of the prism was optically matched to a gold (Au)-coated glass slide cover slip on one side, which would act as the sensing layer, while a customized chamber was pressed onto the other side of the cover slip. The intensity of the reflected laser beam from the base of the prism was detected by a photodetector (Thorlabs, PDA100A) and then amplified using a lock-in amplifier (Stanford Research, SR530) prior to computer analysis using Matlab software.

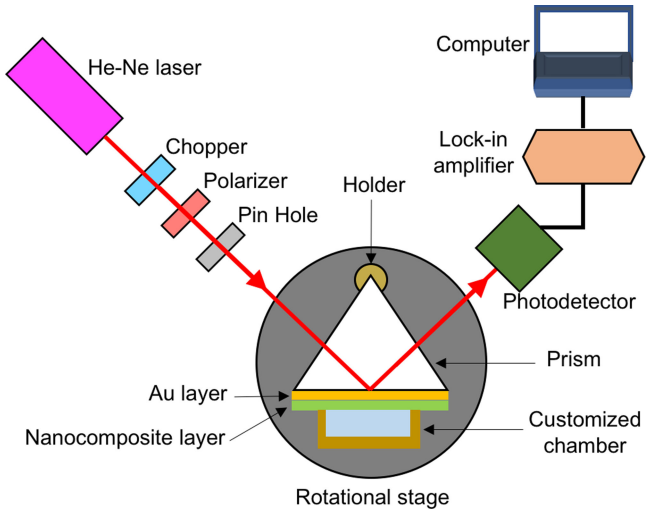


Fig. 1. Experimental setup of SPR with static water chamber.

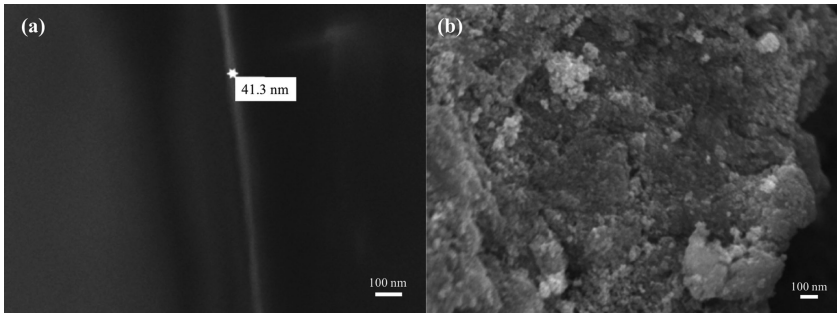


Fig. 2. FESEM image of (a) gold layer thickness and (b) rGO/$\gamma$-$Fe_2O_3$ powder deposited on the glass slide.

## 3. Fabrication of Sensing Layer

The sensing layer was prepared on a 22 $\times$ 22 mm microscopic glass slide coverslip (Deckglasser) which was attached to the prism using an index-matching liquid with viscosity of 100 cps. Firstly, Au layer was deposited onto the coverslip in order to generate the plasmonic effect. The deposition was conducted using a sputter coater (K575X from Quorum Technologies) under room temperature which yielded a thickness of 41.3 nm when analyzed using field-effect scanning electron microscopy (FESEM) as shown in Fig. 2(a). Similar thickness of Au layer was also reported in previous literature for optimum performance [15].

For the deposition of rGO/$\gamma$-$Fe_2O_3$, its solution was firstly prepared by adding 0.1 g of the composite material in powdered form, obtained from [16], into 10 ml of pure ethanol. The solution was sonicated for 10 minutes. After sonication, the mixture was coated using an airbrush and the coverslip was heated on a hotplate at 80 °C, simultaneously. The pressure of airbrush was set at 21 PSI and the air output was maintained 15 l/minute in order to obtain a consistent homogenous coating. The thickness of rGO/$\gamma$-$Fe_2O_3$ was optimized by preparing 6 sensing layers with varied spraying times of rGO/$\gamma$-$Fe_2O_3$ within the range of 40 s to 90 s and measuring the angle resonance shift of each prepared sensing layer as they were introduced to 5 ppm of $Pb^{2+}$. The largest shift was obtained with spraying time of 70 s that corresponded to a thickness of $\sim$9 nm when simulated using Fresnel's equations for multilayer systems [17].

The surface was analyzed using FESEM as depicted in Fig. 2(b). From this FESEM image, dark spots indicating the presence of rGO were observed to be scattered on the glass surface with

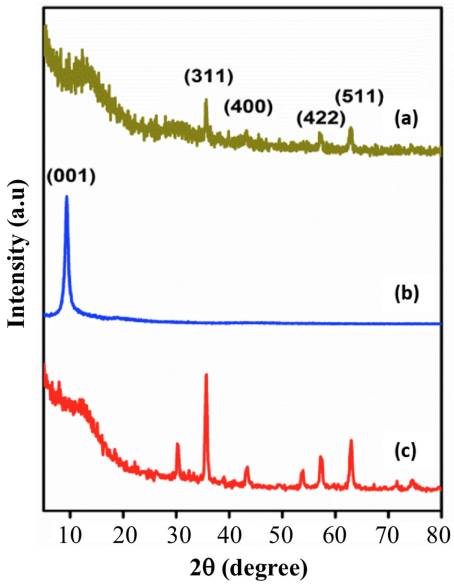


Fig. 3. XRD spectrum of (a) rGO, (b) $Fe_2O_3$, and (c) rGO/$\gamma$-$Fe_2O_3$.

intermittent appearance of white clusters which represents the $Fe_2O_3$ matrix. The image validates the presence of the nanocomposite on the surface of the coverslip.

Fig. 3 shows the x-ray diffraction (XRD) analysis of the materials used in this research work. From Fig. 3(c), band peaks obtained from the surface are incoherent with reference peaks taken for rGO and $Fe_2O_3$, individually, [see Fig. 3(a) and (b)]. For rGO/$\gamma$-$Fe_2O_3$ sample, the characteristic peaks of $Fe_2O_3$ such as (311), (400), (422), (511) can be seen, while the (001) plane peak of GO becomes broad and its intensity becomes weak. The peak of GO is similar to the one reported in [18]. The phenomenon of broadening peak is also confirmed in other published article, which reports that the sharp diffraction peaks turn weak or even vanish signifying the collapse of the GO layers [19].

Next, the coverslip was immersed in EDC/NHS solution, which was prepared by mixing 50 mol of EDC and 50 mol of NHS. The purpose of introducing EDC/NHS to the process of building the sensing layer is to activate the carboxylic acid grounds on both the edges and the basal plane of the rGO so that the integrity of the compound is maintained on the surface of the coverslip [20]. After approximately 15 minutes of immersion time at a fixed temperature of $\sim$3 °C, the coverslip was rinsed with DI water gently and left to dry for 10–15 minutes before it was attached onto the prism [21]. The thickness of the EDC/NHS layer was determined using Fresnel's equations on multilayer systems as well [17], which obtained a thickness of 4 nm.

Fig. 4 shows the Fourier-transform infrared spectroscopy (FTIR) spectra of rGO/$\gamma$-$Fe_2O_3$ and rGO/$\gamma$-$Fe_2O_3$-EDC/NHS. In Fig. 4(a), the broad peak presented within the range of 3000–3500 $cm^{-1}$ is ascribed to the stretching of O–H of intercalated water. The absorption peaks from 1727 $cm^{-1}$ and 1610 $cm^{-1}$ can be assigned to C=O stretching vibrations of carboxylic functional groups while band peak at 1030.43 $cm^{-1}$ represents C–O stretching vibration of epoxide. The observed peaks in rGO/$\gamma$-$Fe_2O_3$ confirm the presence of oxygen-functional groups in carbon framework. Also, a band peak at 2917.39 $cm^{-1}$ is observed before the introduction of EDC/NHS which represents the carboxyl group on rGO-COOH. However, the peak is absent when EDC/NHS was introduced and a new band peak appeared at 1516.30 $cm^{-1}$ as depicted in Fig. 4(b) representing the covalent bond formed between EDC/NHS and carboxyl groups. These findings indicate that the addition of EDC/NHS into the rGO/$\gamma$-$Fe_2O_3$ chemical structure enables stronger covalent bonds that permit it to sustain the original chemical structure.

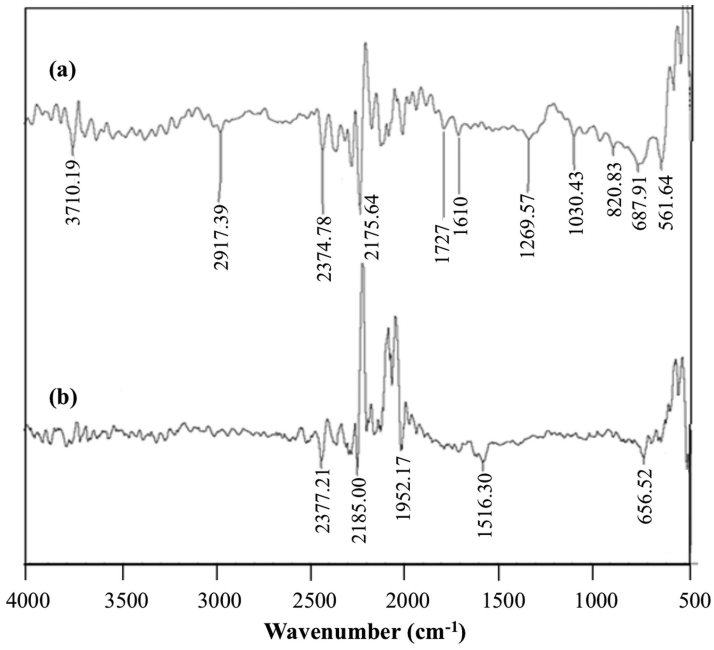


Fig. 4. FTIR spectrum of (a) Au/rGO/$\gamma$-$Fe_2O_3$ and (b) Au/rGO/$\gamma$-$Fe_2O_3$-EDC/NHS.

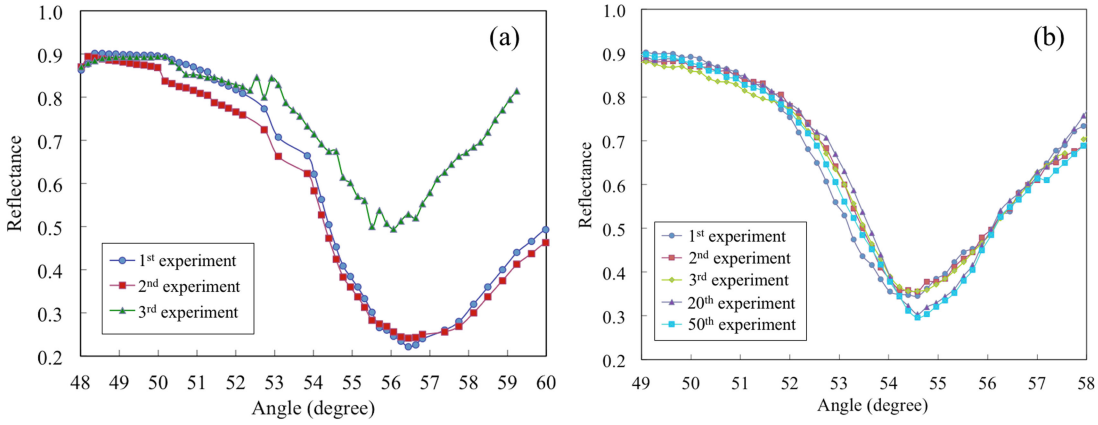


Fig. 5. SPR curves of Au-rGO/$\gamma$-$Fe_2O_3$ (a) without EDC/NHS, and (b) with EDC/NHS.

## 4. Reliability Test of EDC/NHS Coated Sensor Chip

In order to justify the impact of EDC/NHS, a proper comparison was made between the EDC/NHS coated sensor chip and the conventional bilayer sensor chip of Au-rGO/$\gamma$-$Fe_2O_3$. This was conducted by using the same configuration with DI water as sample. The sample was inserted into the sample chamber and was left for 15 minutes before measurements were taken. The procedure was repeated until the signal deviated or became unstable. From Fig. 5(a), the deterioration of the SPR signal is clearly observed after the third set of experiment. The resonance dip decreases after each consequent set and the signal quality became poorer. This may be attributed to the weak van der Waals force between the graphene layers which led to deterioration when rGO/$\gamma$-$Fe_2O_3$ layer interacted with water molecules [22], [23]. On the other hand, the EDC/NHS layer produced a more reliable SPR signal even after 50 sets of experiments as depicted in Fig. 5(b). It can be observed that after the 20$^{th}$ experiment and onwards, the resonance angle shifted by a small angle of 0.185° and the SPR signal quality was preserved surpassing the 50$^{th}$ experiment. From these

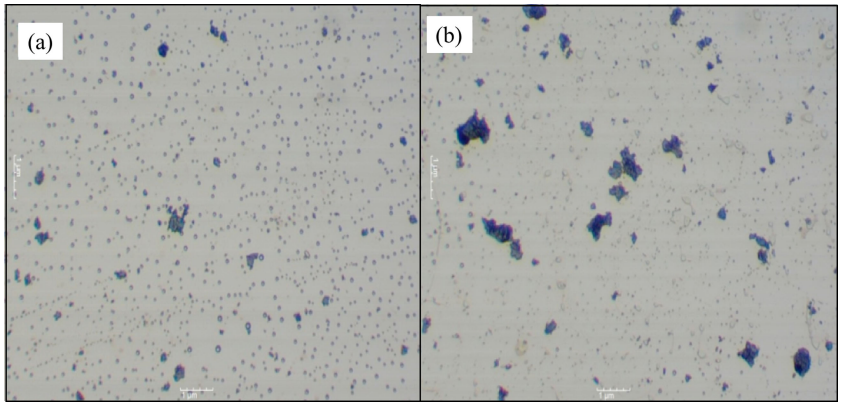


Fig. 6. Microscopic images at a 1 $\mu$m scale show the effect of water on (a) rGO/$\gamma$-$Fe_2O_3$ and (b) rGO/$\gamma$-$Fe_2O_3$-EDC/NHS.

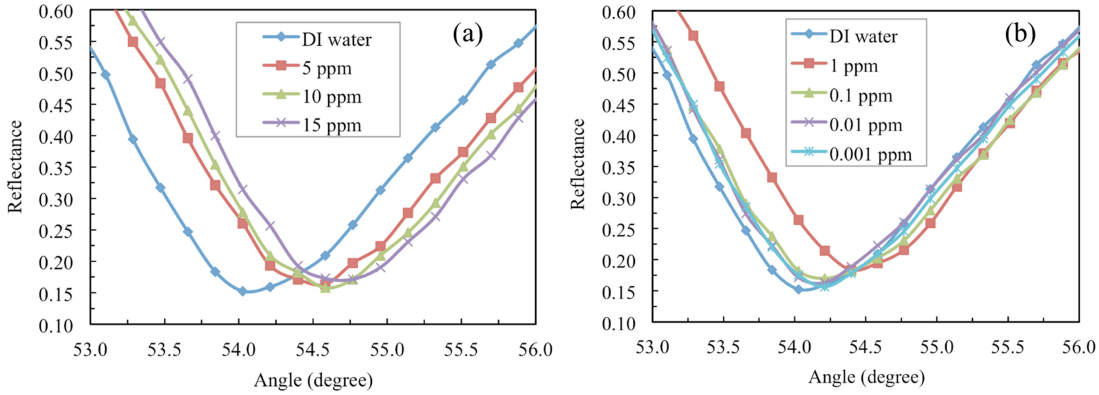


Fig. 7. Measured SPR signal for different $Pb^{2+}$ ion concentrations within the range of (a) 5–15 ppm and (b) 0.001–1 ppm.

two findings, EDC/NHS did manage to promote better adhesion between graphene layers which allowed the same sensor chip to be used multiple times without showing any significant degradation of signal quality.

Fig. 6(a) and (b) show microscopic images of the graphene-based sensor with and without EDC/NHS after testing with deionized (DI) water, respectively. By comparing these figures, the count of graphene flakes is larger for the case with EDC/NHS as depicted in Fig. 6(b). In addition to that, micro bubbles can be clearly seen from Fig. 6(a). The formation of micro-bubbles indicates the presence of trapped air in the sensing layer which impaired the sensing performance. Therefore, without any protection layer, the rGO/$\gamma$-$Fe_2O_3$ nanocomposite cannot sustain its physical form for multiple experiments with aqueous sample.

## 5. Sensing Performance

The SPR sensor chip that had been coated with EDC/NHS was introduced to different concentrations of $Pb^{2+}$ in DI water within the range of 5 to 15 ppm, at an interval of 5 ppm. Exposure time was fixed at 25 minutes. From Fig. 7(a), a consistent angle shift to the right can be observed as the concentration increases. At 5 ppm of $Pb^{2+}$, an angle shift of 0.55° was yielded from the reference curve, while 15 ppm produced an angle shift of 0.74°. However, no difference in SPR resonance angle was noted between concentrations of 5 ppm and 10 ppm. This was due to the limitation of the SPR setup that had a minimum rotational angle fixed at 0.184°. The rate of change

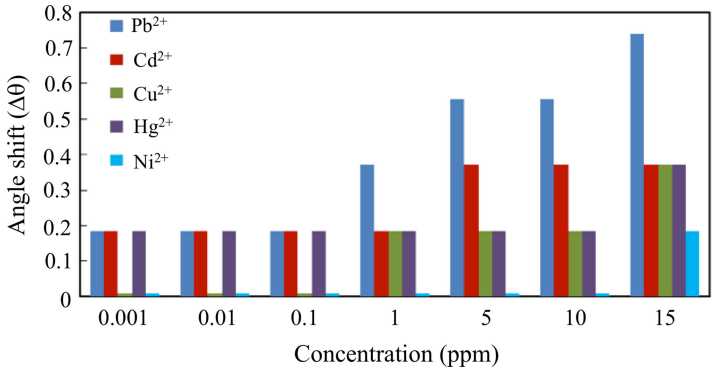


Fig. 8. Measured resonance angle shift with different heavy metals at varying concentrations.

within the range of 5 ppm to 15 ppm and 0 ppm to 5 ppm were calculated to be 0.0184°/ppm and 0.1112°/ppm, respectively. The rate difference between the two concentration ranges was attributed to the availability of binding sites on the sensing layer. When high concentration of Pb ions were introduced (5 ppm to 15 ppm), most of the active sites would be occupied with the analyte which regressed the capacity of the sensing layer to accommodate more Pb ions. Thus, despite further increment in analyte concentration within the stated range, the net interaction was small which had led to a slower rate. On the contrary, the minimal interaction of analyte at low concentration of Pb ions (0 ppm to 5 ppm) would have left more available active sites on the sensing layer. Hence, the sensing layer maintained its capacity to accommodate further absorption of Pb ions which resulted to a larger net interaction and a higher rate. The same observation was reported in [24]–[26].

From these findings, the developed SPR sensor has higher sensitivity for $Pb^{2+}$ ion concentrations below 5 ppm. Further tests were carried out with $Pb^{2+}$ within the concentration range of 0.001 ppm to 1 ppm. In Fig. 7(b), a consistent red shift can be observed again as the concentration increases. Angle shift of 0.368° was yielded when 1 ppm of $Pb^{2+}$ was introduced, while the remaining concentrations which were tested (0.1, 0.01, and 0.001 ppm) remained at an angle shift of 0.184°. The LOD for the SPR sensor was found to be 0.001 ppm, which is on par with what was reported in [27]. The observed resonance angle shift supports the occurrence of $Pb^{2+}$ absorption onto the rGO/$\gamma$-$Fe_2O_3$ sensing layer. This can be mainly attributed to the ionization of the hydroxyl groups present on the rGO/$\gamma$-$Fe_2O_3$ surface under the influence of the $Pb^{2+}$ solvent's neutral pH state [13], [28]. In return, a mass transfer driving force is created which enhances the interaction and adsorption of $Pb^{2+}$ onto the sensing layer.

The rGO/$\gamma$-$Fe_2O_3$ sensing layer was also tested with different heavy metal ions to gauge its selectivity towards $Pb^{2+}$ ion. In this experiment, the designed SPR sensor was exposed to other heavy metal ions; $Cd^{2+}$, $Cu^{2+}$, $Hg^{2+}$ and $Ni^{2+}$ at concentrations ranging from 0.001 to 15 ppm. The SPR signal was taken for 25 minutes to ensure that the interaction between rGO/$\gamma$-$Fe_2O_3$ sensing layer and analytes was maximized. Each type of ions was measured individually and all results were collected as shown in Fig. 8.

At 0.001, 0.01 and 0.1 ppm, the rGO/$\gamma$-$Fe_2O_3$ nanomaterial was sensitive towards $Pb^{2+}$, $Cd^{2+}$ and $Hg^{2+}$ with angle shift of 0.185°. Within this concentration range, the sensor was not able to distinguish between these heavy metals due to the limited rotational angle of the setup. For concentrations above 1 ppm, the SPR sensor exhibited higher sensitivity towards $Pb^{2+}$ ions. These results indicate that the rGO/$\gamma$-$Fe_2O_3$ sensing layer is an effective nanomaterial to detect $Pb^{2+}$ ions at minimum concentration of 1 ppm.

## 6. Limit of Detection Enhancement

Based on the previous experiments, the LOD for the developed sensor; Au-rGO/$\gamma$-$Fe_2O_3$ protected by EDC/NHS was limited to 0.001 ppm of $Pb^{2+}$ ion. In order to enhance the LOD to sub-ppb, a

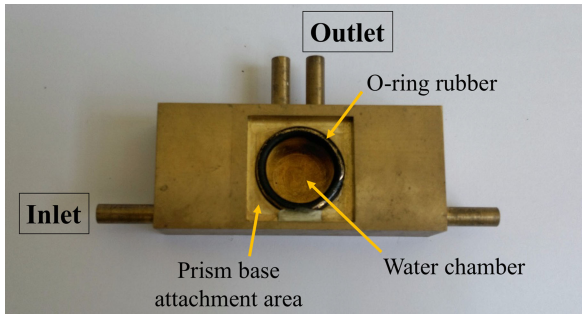


Fig. 9. Custom-made water circulation chamber to enhance $Pb^{2+}$ ion limit of detection.

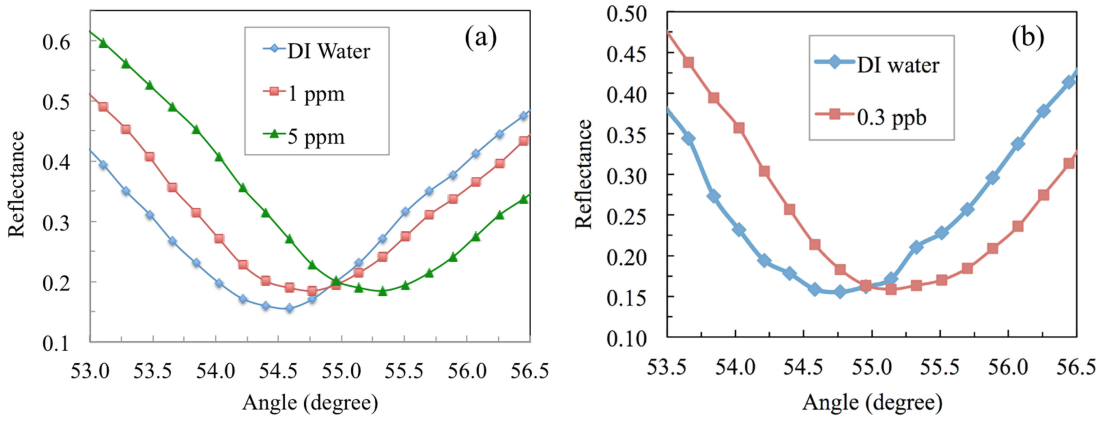


Fig. 10. Measured SPR signal from water circulation experiment at $Pb^{2+}$ ion concentration of (a) 1 ppm and 5 ppm, and (b) 0.3 ppb.

water circulation design was adapted in this work in order to increase the interaction rate between the sample and the sensing layer. To perform this experiment, a custom-made brass alloy chamber was made as depicted in Fig. 9. Four inlet/outlet ports were included in the design to allow the manipulation of water entrance point and flow direction within the chamber. The water chamber (circular compartment) had a corresponding diameter and depth of 20 and 13 mm with opening for the prism at the side of the chamber. Although the water chamber had four total ports, only a pair of ports was used for the prism-based SPR experiment while the other two ports were concealed with clay to prevent any water leakage. The inlet and outlet were connected to a 1000 $cm^3$ water container and DC water pump using plastic pipes. In order to maximize the interaction between the analyte and sensing layer, a 90° angle between the inlet and outlet was chosen to allow the chamber to be completely filled up with the liquid sample.

The sensing mechanism in heavy metals depends on the adsorption of ions by the sensing surface. The perfect condition for this experiment is to have a laminar flow which would increase the interaction between heavy metal ions and sensing surface [29]. However, high flow rate may lead to the presence of turbulence and vortex, which could destabilize the sensing interaction and change the spatial concentration of analyte. Based on preliminary studies with 5 ppm concentration of $Pb^{2+}$ ions, the optimum flow rate to get the maximum angle shift was recorded at 0.21 l/minute flow rate and this value was fixed throughout the remaining experiments.

The sensing performance of the newly adapted configuration with water circulation was analyzed with $Pb^{2+}$ at concentrations 1 ppm and 5 ppm. The experimental results for these concentrations are portrayed in Fig. 10(a). From these findings, the angle shifts for 1 and 5 ppm were 0.368° and 0.736°, respectively. Both values indicated the enhancement of angle shift by 0.184° when compared to static water. Furthermore, the measurement time was reduced to 6 minutes which was 4 times faster

than the detection method in static condition. These findings prove that the diffusion of $Pb^{2+}$ ions into the sensing layer was enhanced with the implementation of water circulation. The LOD for the water circulation SPR sensor configuration was further analyzed by testing $Pb^{2+}$ from 0.1 to 0.9 ppb at the interval of 0.2 ppb. The time of detection was fixed at 6 minutes. The lowest concentration detected was 0.3 ppb which resulted in an angle shift of 0.368°, as depicted in Fig. 10(b). To the best of our knowledge, this is by far the lowest LOD achieved for the detection of $Pb^{2+}$ using an SPR-based sensor.

## 7. Conclusion

The work has successfully demonstrated rGO/$\gamma$-$Fe_2O_3$ as a sensing layer to an SPR sensor for the detection of $Pb^{2+}$ in water. The sensing performance of the sensor is not only comparable to the recent studies listed in Table 1, it also has the lowest LOD at 0.3 ppb with a sensing time of $\sim$6 minutes. EDC/NHS was added onto the sensing layer to increase the integrity of the sensing surface. This enabled the sensor to withstand its performance during multiple tests without any significant deviation. The sensor also showed good specificity of $Pb^{2+}$ at concentrations 1 ppm and above. Overall, the SPR sensor has shown to be a highly viable tool for fast, sensitive and selective detection of $Pb^{2+}$ in water.

## References


[1] World Health Organization, "Lead poisoning and health," 2017. [Online]. Available: http://www.who.int/mediacentre/factsheets/fs379/en/

[2] J. Yan and E. M. Indra, "Colorimetric method for determining $Pb^{2+}$ ions in water enhanced with non-precious-metal nanoparticles," *Anal. Chem.*, vol. 84, no. 14, pp. 6122–6127, 2012.

[3] N. F. Lokman *et al.*, "Highly sensitive SPR response of Au/chitosan/graphene oxide nanostructured thin films toward Pb (II) ions," *Sens. Actuators B, Chem.*, vol. 195, pp. 459–466, 2014.

[4] M. Li *et al.*, "Red shift of side-polished fiber surface plasmon resonance sensors with silver coating and inhibition by gold plating," *IEEE Photon. J.*, vol. 9, no. 3, Jun. 2017, Art. no. 7103913.

[5] S. Hayashi, D. V Nesterenko, A. Rahmouni, and Z. Sekkat, "Observation of Fano line shapes arising from coupling between surface plasmon polariton and waveguide modes," *Appl. Phys. Lett.*, vol. 108, no. 5, 2016, Art. no. 51101.

[6] L. Yang, J. Wang, L. Yang, Z.-D. Hu, X. Wu, and G. Zheng, "Characteristics of multiple Fano resonances in waveguide-coupled surface plasmon resonance sensors based on waveguide theory," *Sci. Rep.*, vol. 8, no. 1, 2018, Art. no. 2560.

[7] G. Zheng, J. Cong, L. Xu, and J. Wang, "High-resolution surface plasmon resonance sensor with Fano resonance in waveguide-coupled multilayer structures," *Appl. Phys. Exp.*, vol. 10, no. 4, 2017, Art. no. 042202.

[8] Z. Sekkat *et al.*, "Plasmonic coupled modes in metal-dielectric multilayer structures: Fano resonance and giant field enhancement," *Opt. Exp.*, vol. 24, no. 18, pp. 20080–20088, 2016.

[9] A. R. Sadrolhosseini, A. S. M. Noor, A. Bahrami, H. N. Lim, Z. A. Talib, and M. A. Mahdi, "Application of polypyrrole multi-walled carbon nanotube composite layer for detection of mercury, lead and iron ions using surface plasmon resonance technique," *PLoS One*, vol. 9, no. 4, 2014, Art. no. e93962.

[10] N. H. Kamaruddin, A. A. A. Bakar, N. N. Mobarak, M. S. D. Zan, and N. Arsad, "Binding affinity of a highly sensitive au/ag/au/chitosan-graphene oxide sensor based on direct detection of $Pb^{2+}$ and $Hg^{2+}$ ions," *Sensors*, vol. 17, no. 10, 2017, Art. no. 2277.

[11] A. M. Shrivastav, S. P. Usha, and B. D. Gupta, "Optical fiber SPR sensor for simultaneous determination of Cu(II) and Pb(II) ions using molecular imprinting," in *Proc. Int. Conf. Frontiers Opt.*, 2016, Paper JTh2A.53.

[12] N. H. Kamaruddin, N. M. A. Jamaludin, N. F. Lokman, and A. A. A. Bakar, "Effect of bi-metallic structure on the performance of chitosan-graphene oxide surface plasmon resonance sensor," in *Proc. 5th Int. Conf. IEEE Photon.*, 2014, pp. 185–187.

[13] S. Kumar, R. R. Nair, P. B. Pillai, S. N. Gupta, M. A. R. Iyengar, and A. K. Sood, "Graphene oxide-$MnFe_2O_4$ magnetic nanohybrids for efficient removal of lead and arsenic from water," *ACS Appl. Mater. Interfaces*, vol. 6, no. 20, pp. 17426–17436, 2014.

[14] D. Fialova *et al.*, "Interaction of heavy metal ions with carbon and iron based particles," *Materials*, vol. 7, no. 3, pp. 2242–2256, 2014.

[15] D. Yang, H-H. Lu, B. Chen, and C-W. Lin, "Surface plasmon resonance of $SnO_2$/Au bi-layer films for gas sensing applications," *Sens. Actuators B, Chem.*, vol. 145, no. 2, pp. 832–838, 2010.

[16] T. Peik-See, A. Pandikumar, H. Ngee, and N. Ming, "Magnetically separable reduced graphene oxide/iron oxide nanocomposite materials for environmental remediation," *Catal. Sci. Technol.*, vol. 4, pp. 4396–4405, 2014.

[17] K. Matsubara, S. Kawata, and S. Minami, "Multilayer system for a high-precision surface plasmon resonance sensor," *Opt. Lett.*, vol. 15, no. 1, pp. 75–77, 1990.

[18] Z. Wang, C. Ma, H. Wang, Z. Liu, and Z. Hao, "Facilely synthesized $Fe_2O_3$–graphene nanocomposite as novel electrode materials for supercapacitors with high performance," *J. Alloys Compound*, vol. 552, pp. 486–491, 2013.

[19] C. Fu, G. Zhao, H. Zhang, and S. Li, "Evaluation and characterization of reduced graphene oxide nanosheets as anode materials for lithium-ion batteries," *Int. J. Electrochem. Sci.*, vol. 8, no. 5, pp. 6269–6280, 2013.
[20] N. Chiu, T. Huang, and H. Lai, "Graphene oxide based surface plasmon resonance biosensors," in *Advances in Graphene Science*, M. Aliofkhazraei, ed. London, U. K.: IntechOpen, 2013.
[21] S. Roy, N. Soin, R. Bajpai, D. S. Misra, J. A. McLaughlin, and S. S. Roy, "Graphene oxide for electrochemical sensing applications," *J. Mater. Chem.*, vol. 21, no. 38, pp. 14725–14731, 2011.
[22] R. Huang, "Graphene: Show of adhesive strength," *Nat. Nanotechnol.*, vol. 6, no. 9, pp. 537–538, 2011.
[23] H. S. Dong and S. J. Qi, "Realising the potential of graphene-based materials for biosurfaces—A future perspective," *Biosurf. Biotribol.*, vol. 1, no. 4, pp. 229–248, 2015.
[24] Z. Wu *et al.*, "Room temperature methane sensor based on graphene nanosheets/polyaniline nanocomposite thin film," *IEEE Sensors J.*, vol. 13, no. 2, pp. 777–782, Feb. 2013.
[25] S. Usha, S. Mishra, and B. Gupta, "Fabrication and characterization of a SPR based fiber optic sensor for the detection of chlorine gas using silver and zinc oxide," *Materials*, vol. 8, no. 5, pp. 2204–2216, 2015.
[26] D. K. Roper, "Determining surface plasmon resonance response factors for deposition onto three-dimensional surfaces," *Chem. Eng. Sci.*, vol. 62, no. 7, pp. 1988–1996, 2007.
[27] A. Hynninen, K. Tõnismann, and M. Virta, "Improving the sensitivity of bacterial bioreporters for heavy metals," *Bioeng. Bugs*, vol. 1, no. 2, pp. 132–138, 2010.
[28] N. T. V. Hoan, N. T. A. Thu, H. Van Duc, N. D. Cuong, D. Q. Khieu, and V. Vo, "$Fe_3O_4$/reduced graphene oxide nanocomposite: Synthesis and its application for toxic metal ion removal," *J. Chem.*, vol. 2016, 2016, Art. no. 2418172.
[29] T. Gervais and K. F. Jensen, "Mass transport and surface reactions in microfluidic systems," *Chem. Eng. Sci.*, vol. 61, no. 4, pp. 1102–1121, 2006.